The FcεRI signaling cascade and integrin trafficking converge at patterned ligand surfaces

Devin L. Wakefield†, David Holowka, and Barbara Baird*
Department of Chemistry and Chemical Biology, Cornell University, Ithaca, NY 14853

ABSTRACT **We examined the spatial targeting of early and downstream signaling mediated by the immunoglobulin E (IgE) receptor (FcεRI) in RBL mast cells using surface-patterned 2,4-dinitrophenyl (DNP) ligands. Micron-sized features of DNP are presented as densely immobilized conjugates of bovine serum albumin (DNP-BSA) or mobile in a supported lipid bilayer (DNP-SLB). Although soluble anti-DNP IgE binds uniformly across features for both pattern types, IgE bound to FcεRI on cells shows distinctive distributions: uniform for DNP-SLB and edge concentrated for DNP-BSA. These distributions of IgE-FcεRI propagate to the spatial recruitment of early signaling proteins, including spleen tyrosine kinase (Syk), linker for activation of T-cells (LAT), and activated phospholipase C gamma 1 (PLCγ1), which all localize with engaged receptors. We found stimulated polymerization of F-actin is not required for Syk recruitment but is progressively involved in the recruitment of LAT and PLCγ1. We further found β1- and β3-integrins colocalize with IgE-FcεRI at patterned ligand surfaces as cells spread. This recruitment corresponds to directed exocytosis of recycling endosomes (REs) containing these integrins and their fibronectin ligand. Together our results show targeting of signaling components, including integrins, to regions of clustered IgE-FcεRI in processes that depend on stimulated actin polymerization and outward trafficking of REs.**

Monitoring Editor
Diane Lidke
University of New Mexico

Received: Apr 3, 2017
Revised: Jul 18, 2017
Accepted: Jul 31, 2017

INTRODUCTION

The high-affinity receptor for immunoglobulin E (IgE), FcεRI, serves as a model immunoreceptor that mediates cell activation in response to antigenic ligands. Ligand-induced aggregation of IgE-FcεRI complexes on the surface of basophils and mast cells initiates a complex biochemical signaling cascade, resulting in specific cellular responses (Rivera and Gilfillan, 2006). Studied extensively in RBL mast cells (and to a lesser extent in bone marrow–derived and other mast cells), the signaling pathway proceeds with tyrosine kinase Lyn of the Src family, which is anchored to the inner leaflet of the plasma membrane. Lyn phosphorylation of immunoreceptor tyrosine–based activation motifs on FcεRI β and γ subunits results in recruitment and activation of the cytoplasmic spleen tyrosine kinase (Syk) of the Syk/Zap-70 family. Syk phosphorylates the scaffold protein linker for activation of T-cells (LAT) along with several other substrates that coassemble in signaling complexes. Multiple downstream signaling pathways emanate from adaptor proteins that bind to phosphorylated LAT, including SLP76, which associates with LAT via adaptor Gads, and further binds to adaptor protein Nck and to phospholipase C gamma 1 (PLCγ1), among other proteins (Koretzky *et al.*, 2006). Recruitment of Nck leads to nucleation of F-actin via the WASP-Arp2/3 pathway. LAT-recruited PLCγ1 is activated by Bruton's tyrosine kinase to hydrolyze phosphatidylinositol-4,5-bisphosphate (PIP_2) to inositol 1,4,5-trisphosphate (IP_3) and 2,3-diacylglycerol (DAG) (Barker *et al.*, 1998). These PLCγ1 hydrolysis products act as second messengers in protein kinase C activation and Ca^{2+} mobilization, culminating in exocytotic release of secretory granules (degranulation) and other mast cell responses (Holowka *et al.*, 2012; Gaudenzio *et al.*, 2016).

This article was published online ahead of print in MBoC in Press (http://www.molbiolcell.org/cgi/doi/10.1091/mbc.E17-03-0208) on August 9, 2017.

†Present address: Department of Molecular Medicine, Beckman Research Institute of the City of Hope Comprehensive Cancer Center, Duarte, CA 91010.

*Address correspondence to: Barbara Baird (bab13@cornell.edu).

Abbreviations used: A488, Alexa Fluor 488; BSA, bovine serum albumin; BSS, balanced salt solution; CTxB, cholera toxin subunit B; CytoD, cytochalasin D; DAG, 2,3-diacylglycerol; DNP, 2,4-dinitrophenyl; ECM, extracellular matrix; FBS, fetal bovine serum; FcεRI, IgE receptor; FITC, fluorescein isothiocyanate; FN, fibronectin; GMBS, N-(γ-maleimidobutyryloxy)succinimide ester; IgE, immunoglobulin E; IgG, immunoglobulin G; IP_3, inositol 1,4,5-trisphosphate; LAT, linker for activation of T-cells; MPTS, 3-mercaptopropyl)trimethoxysilane; PBS, phosphate-buffered saline; PIP_2, phosphatidylinositol-4,5-bisphosphate; PLCγ1, phospholipase C gamma 1; RE, recycling endosome; Rhod-FN, rhodamine-fibronectin; ROI, region of interest; SLB, supported lipid bilayer; SUV, small unilamellar vesicle; Syk, spleen tyrosine kinase; VLA-4, very late antigen-4; YFP, yellow fluorescent protein.

Stimulated signaling events in mast cells are accompanied by morphological changes, characterized in RBL cells by increased spreading on a surface and membrane ruffling, which both involve reorganization of the actin cytoskeleton (Apgar, 1991). In general, the cytoskeleton plays multiple intricate roles in cellular maintenance of homeostasis and responses to specific environmental signals. Cytochalasin D (CytoD) and latrunculin, which inhibit actin polymerization, have been used to investigate these various roles as related to specific functions, including organization of lipid domains (Pierini *et al.*, 1996; Holowka *et al.*, 2000; Shelby *et al.*, 2016), phosphorylation of signaling components (Frigeri and Apgar, 1999; Holowka *et al.*, 2000), and receptor mobility (Andrews *et al.*, 2008). A number of signaling proteins engaged after activation of FcεRI have been characterized as contributing to stimulated actin cytoskeleton responses in mast cells (Draber *et al.*, 2012). Despite these studies, the multifaceted regulation of FcεRI-mediated signaling activities by F-actin remains poorly defined, and progress depends on pinpointing specific roles.

Mast cells interact with other cells and surfaces in their physiological environment, mediated in part by transmembrane integrin proteins (Metcalfe *et al.*, 1997). FcεRI-mediated signaling was shown to up-regulate the activity of the integrin VLA-4 (α4β1) in mast cells (Hernandez-Hansen *et al.*, 2004), and VLA-4 and LFA-1 (αLβ2) integrins are involved in functional conjugation to dendritic cells (Carroll-Portillo *et al.*, 2015). These two integrins are expressed on several types of mast cells, and LFA-1 has been characterized as a key participant in chemotaxis to sites of inflammation (Weber *et al.*, 1997). Furthermore, engagement of integrins on mast cells with their ligands on adjoining target cells has been shown to enhance FcεRI-mediated signaling activities and polarize mast cell exocytosis in the direction of the target cell (Joulia *et al.*, 2015). However, relatively little is known about the dynamic display of mast cell–surface integrin activity and the spatial distribution with respect to sites of ligand stimulation.

Integrins VLA-4 (α4β1), VLA-5 (α5β1), and VNR (αvβ3) have been characterized on RBL and rat peritoneal mast cells and are shown to bind extracellular matrix (ECM) proteins fibronectin (FN), vitronectin, and fibrinogen (Yasuda *et al.*, 1995). VLA-5 targets the cell-binding domain recognition sequence (RGD) of FN and VLA-4 binds the CS-1 sequence (LDV) on the type III connecting segment of FN (Yamada, 1991). Mast cells adhere and spread on surfaces coated with either FN (Hamawy *et al.*, 1992; Apgar, 1997) or with antibodies specific for integrins (Yasuda *et al.*, 1995). These processes are mediated by integrin–ligand binding and cytoskeletal reorganization and cause markedly enhanced signaling activities and degranulation when stimulated by soluble ligand for IgE-FcεRI.

Here we examine the interplay of the actin cytoskeleton with FcεRI-mediated signaling activities of Syk, LAT, and PLCγ1 in RBL mast cells, and we find progressive dependence on stimulated actin polymerization. We use a surface-patterned ligand approach (Orth *et al.*, 2003) with which we previously demonstrated coclustering of Lyn, F-actin (Wu *et al.*, 2004), and focal adhesion proteins (Torres *et al.*, 2008) with ligand-clustered IgE-FcεRI. We show that β1-containing integrins, including VLA-4, cocluster with activated FcεRI at patterned ligand sites. Further, our experiments reveal that this accumulation depends on stimulated outward trafficking of recycling endosomes and codelivery of integrins with FN ligand. Our results provide new information about the mechanisms by which stimulated actin polymerization and integrin trafficking organize specific signaling responses in migrating, adherent, and polarized mast cells.

RESULTS

Ligand presentation determines the distribution of recruited IgE-FcεRI

We prepared patterned ligand surfaces as described previously (Orth *et al.*, 2003; Wu *et al.*, 2004; Torres *et al.*, 2008), using two methods for 2,4-dinitrophenyl (DNP) presentation (see *Materials and Methods* and Supplemental Figure S1). We compared patterned lipid bilayers containing mobile DNP-cap-DPPE (DNP-SLB; Wu *et al.*, 2004) and patterned DNP-BSA immobilized via covalent surface attachment (Torres *et al.*, 2008; Singhai *et al.*, 2014). As expected, soluble anti-DNP IgE, labeled with Alexa Fluor 488 (A488), binds uniformly to these patterned features with high specificity (Figure 1A). The difference in A488 fluorescence intensity between these two methods of DNP presentation is consistent with the difference in estimated DNP surface density, roughly 1.5×10^5 DNP/μm^2 for DNP-SLB surfaces and 8×10^5 DNP/μm^2 for DNP-BSA surfaces.

Incubation of A488-IgE on RBL cells (roughly 2×10^5 FcεRI/cell) with these different substrates causes distinctive receptor reorganization (Figure 1, B and C). For DNP-SLB surfaces, A488-IgE-FcεRI is uniformly distributed across individual patterned features with little fluorescence observed on parts of the cells away from these features (Figure 1B, top). As a control, nearly all A488-IgE-FcεRI fluorescence appears off SLB-patterned features without DNP ligand (Figure 1B, bottom). Optical sectioning revealed that the reduced fluorescence associated with patterned features in this latter case is due to the plasma membrane residing farther away from the focal plane set at the ventral surface.

We observe a different distribution of A488-IgE-FcεRI on RBL cells incubated on surfaces patterned with immobilized DNP-BSA (Figure 1C, top): A488-IgE-FcεRI fluorescence concentrates at the edges of individual patterned features, yielding a "ring" of fluorescence. This response may be attributed to both the density and the static presentation of multivalent DNP-BSA. As established previously, cross-linked IgE-FcεRI becomes immobilized at the plasma membrane (Menon *et al.*, 1986; Andrews *et al.*, 2008; Shelby *et al.*, 2013), and this may in turn create a barrier for additional IgE-FcεRI diffusing into these regions. We tested lower densities of DNP-BSA and observed similar effects, although somewhat less IgE-FcεRI concentration at the edges and somewhat more interior to the cell (e.g., see Supplemental Figure S9). In comparative experiments that follow, we chose to continue with the higher DNP-BSA density because of the clear contrast with the distribution of IgE-FcεRI on DNP-SLB patterns. Patterned BSA (no DNP) caused no apparent change in IgE-FcεRI distributions, such that the corresponding A488 fluorescence appeared uniform across the entire cell adhering to these surfaces (Figure 1C, bottom). This distribution indicates that nonspecific interactions exist between the cell membrane and these protein-patterned features (in contrast with SLB-patterned features; Figure 1B, bottom).

We quantified IgE-FcεRI distributions on the different substrates using a radial analysis method introduced previously (Singhai *et al.*, 2014) and refined as described in *Materials and Methods* and Supplemental Figures S3 and S4. This method calculates the averaged ratio of fluorescence, on-versus-off the patterned feature, including the fluorescence arising from edge ("ring") effects. Moreover, the method can be used to distinguish features associated with the cell middle from those near the cell edges. Radial analysis results shown in Figure 1D support visual observations from imaging many cells on the two different patterned-surface types. A high fluorescence ratio is determined for A488-IgE-FcεRI with cells incubated on DNP-SLB patterns. This is due to the relatively uniform accumulation across

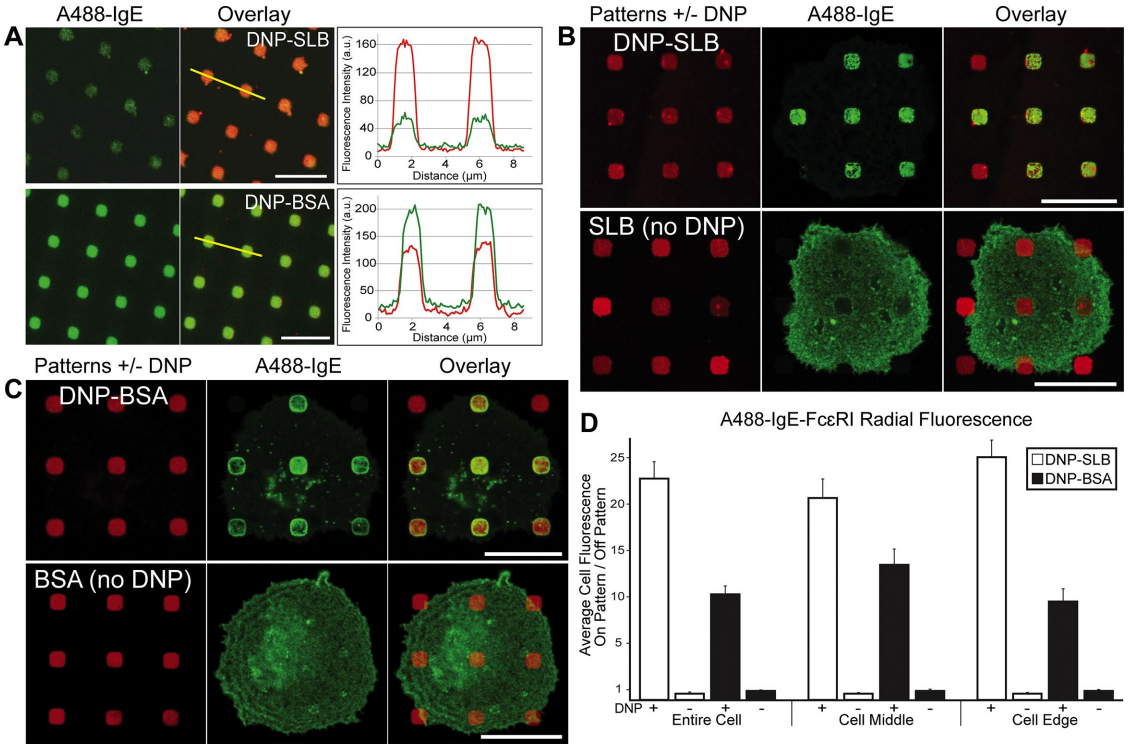

FIGURE 1: A488-IgE–sensitized RBL cells display specific FcεRI clustering on different DNP-patterned surfaces. (A) A488-IgE (green) in solution (5 μg/ml) was incubated with patterned DNP-SLB or DNP-BSA surfaces (red). A line trace across patterned features indicates relative levels of A488-IgE binding to these two types of patterned surfaces (green traces can be directly compared). (B) A488-IgE-sensitized RBL cells were incubated with patterned DNP-SLB (top) or patterned SLB not containing the DNP-cap-DPPE ligand (bottom). (C) A488-IgE–sensitized RBL cells were incubated with patterned DNP-BSA (top) or patterned BSA not conjugated with DNP (bottom). (D) Radial analysis for samples represented in B and C was carried out as described in *Materials and Methods* and Supplemental Figures S3 and S4. The averaged ratio of fluorescence intensity for on-versus-off patterned features was calculated for features across the entire cell or separated into features at the cell edge or cell middle. A value of 1 corresponds to no concentration of fluorescence intensity at patterned features. $N = 25$ cells from three independent experiments for each patterned-surface type. Error bars represent SEM. Scale bars: 5 μm (A); 10 μm (B, C).

features (on) compared with very little fluorescence away from the feature (off) (see Supplemental Figure S3A). In contrast, the fluorescence ratio on-versus-off patterned features is less for the DNP-BSA surfaces. Here the accumulation of A488-IgE-FcεRI apparently reduces diffusion from off-feature regions to the on-feature regions such that a relatively higher level of fluorescence is maintained off patterned features across the cell (see Supplemental Figure S3B).

Syk clusters with patterned DNP ligand independently of F-actin polymerization

We previously observed coclustering of Lyn kinase (Lyn-EGFP) and stimulated tyrosine phosphorylation (4G10 anti-pY mAb; see Supplemental Figure S6B) with IgE-FcεRI in RBL cells at patterned ligand surfaces (Wu *et al.*, 2004). Tyrosines phosphorylated by Lyn on FcεRI γ subunits serve as docking sites for Syk kinase, leading to downstream signaling (Kimura *et al.*, 1996). Using yellow fluorescent protein (YFP)-Syk to assess the spatial organization and extent of intracellular Syk recruitment to the plasma membrane, we found that the distribution of Syk mirrors that observed with A488-IgE-FcεRI on both types of patterned DNP surfaces (compare Figure 2, A and B, with Figure 1, B and C, respectively). Syk association with patterned DNP-SLB regions is uniformly distributed across individual features, whereas Syk localizes at the edges of patterned DNP-BSA features.

We previously showed that CytoD inhibits Lyn recruitment to IgE-FcεRI clustered on similar micron-sized DNP-SLB–patterned features (Wu *et al.*, 2004), consistent with polymerized actin participating in a visibly high level of coaccumulation (Holowka *et al.*, 2000). These studies further showed that IgE-FcεRI accumulation and its catalyzed phosphorylation in the same regions are not inhibited by CytoD, supporting other evidence that recruitment of sufficient Lyn for the initial functional coupling with clustered IgE-FcεRI is mediated within the membrane (Holowka and Baird, 2015). In the present study, we find that the same CytoD treatment on YFP-Syk–expressing cells causes little or no change in Syk recruitment to IgE-FcεRI clustered by patterned DNP ligands (bottom panels in Figure 2, A and B, quantified for multiple cells in Figure 2C), even though F-actin accumulation is dramatically reduced (Supplemental Figure S5B). These results indicate that signaling initiated by clustered IgE-FcεRI does not depend on actin polymerization through the stage of Syk recruitment from the cytoplasm.

LAT colocalizes with clustered IgE-FcεRI at surface-patterned DNP ligand

LAT is a known substrate for Syk, and once phosphorylated, this transmembrane scaffold protein links (directly or indirectly) to PLCγ1 and other proteins to regulate the progression of signaling and Ca^{2+} mobilization in both T-cells (Finco *et al.*, 1998; Zhang *et al.*, 1999)

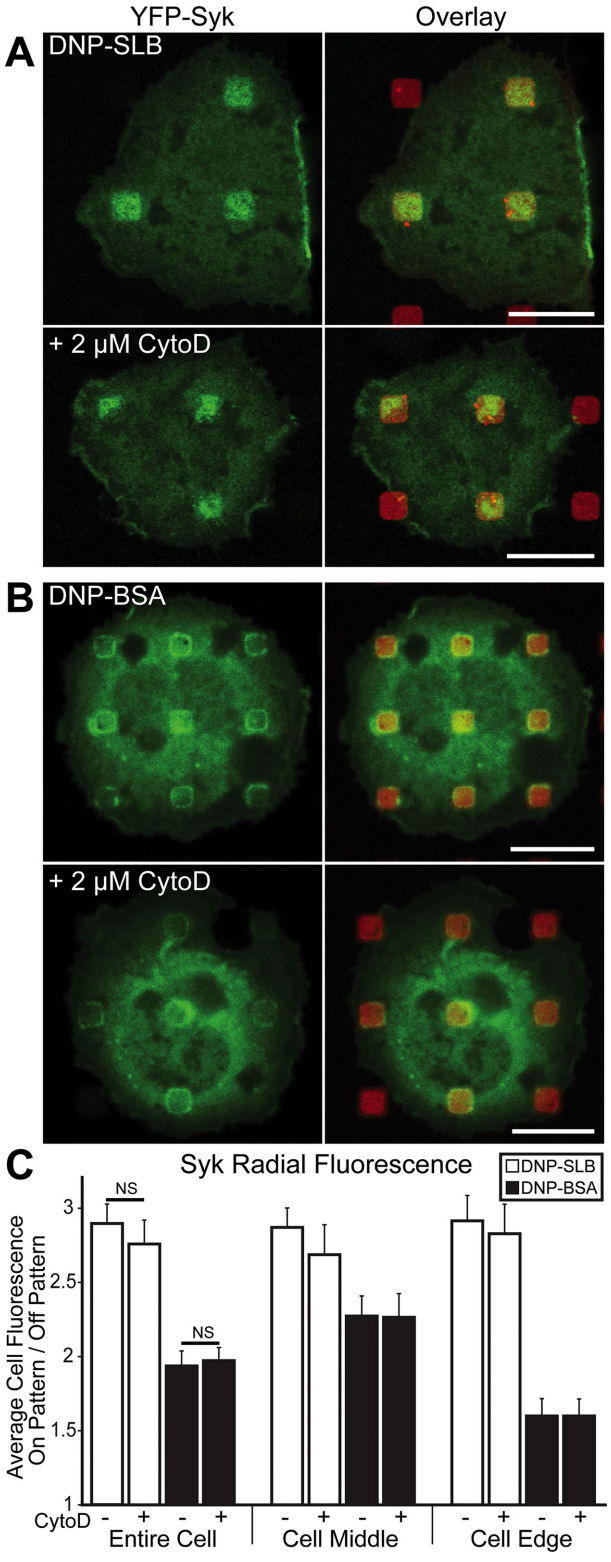

FIGURE 2: Syk kinase stably associates with FcεRI at patterned DNP features, independent of actin polymerization. RBL cells transiently transfected with YFP-Syk (green) and sensitized with IgE were incubated with DNP-SLB (A) or DNP-BSA (B) patterned surfaces (red). Cells shown in bottom panels were pretreated with 2 μM CytoD. (C) Radial analysis was carried out as described in the legend to Figure 1. $N = 24$ cells from three independent experiments for each patterned-surface type. Error bars represent SEM. NS indicates a nonsignificant statistical difference. Scale bars: 10 μm.

and mast cells (Saitoh *et al.*, 2000; Kimura *et al.*, 2001; Silverman *et al.*, 2006). We found that LAT–monomeric enhanced green fluorescent protein (mEGFP) in RBL cells strongly colocalizes with IgE-FcεRI in both types of patterned DNP-ligand surfaces (Figure 3, A and B). These distributions mirror those for IgE-FcεRI and Syk, with LAT-mEGFP recruited more uniformly across DNP-SLB features (Figure 3A, top panels) compared with LAT-mEGFP accumulating largely at the edges of DNP-BSA features (Figure 3B, top panels). For both cases, we observed a similar distribution of LAT recruitment across the cell middle and edges (Figure 3C).

We tested whether actin polymerization participates in LAT coclustering with activated FcεRI, and found that LAT-mEGFP recruitment to patterned DNP-SLB is reduced by ~40% following treatment with CytoD (Figure 3, A and C). In contrast, the same treatment does not reduce LAT-mEGFP association with patterned DNP-BSA (Figure 3, B and C) but maintains a strong level of fluorescence at the edges of individual patterned features. In a separate experiment with patterned DNP-BSA, we investigated LAT activation caused by clustered FcεRI and found that coclustered LAT is specifically phosphorylated. Tyrosine residue 191 (Y191) is one of three Grb2 binding sites on LAT (Zhang *et al.*, 2000), and we observed concentrated levels of anti–phosphoY191 labeling at patterned DNP-BSA sites for 60% of all imaged cells on these surfaces (Figure 3D). The same labeling experiment could not be done reliably with DNP-SLB surfaces, because cell permeabilization conditions used for antibody labeling dissolve the lipid bilayers.

We also evaluated the dynamics of LAT clustering in live RBL cells on DNP-SLB–patterned surfaces. Within 1 min after adding cells, a small region of LAT-mEGFP fluorescence appears in the TIRF field (Figure 3E, left panel, and Supplemental Figure 3E Movie), and the cell continues to spread, with LAT accumulating at patterned features over the next 30 min (Figure 3E, middle panel, and Supplemental Figure 3E Movie). LAT-mEGFP typically displays >80% of its final fluorescence ratio value within the first 5 min of contact with a patterned feature (Figure 3E, right panel, all traces except magenta). After the cell has spread, the off-feature trace (magenta) exhibits a fluorescence ratio of 1, as expected, and the traces for LAT accumulation over DNP-SLB features range from 1.5 to 3.

F-actin polymerization supports PLCγ1 recruitment to patterned DNP-ligands

PLCγ1 is known to interact with LAT complexes activated by immune receptors in mast cells (Saitoh *et al.*, 2000) and T-cells (Zhang *et al.*, 2000), and we found that PLCγ1-EGFP in transfected RBL cells also concentrates in regions of patterned DNP-SLB (Figure 4A, top left two panels) and DNP-BSA (Figure 4A, top right two panels). The spatial organization of PLCγ1 recruitment to patterned DNP sites mirrors the trends observed with Syk, LAT, and FcεRI clustering for DNP-BSA compared with DNP-SLB, in terms of both distributions across respective features and across the cell contact regions. Treating parallel samples with 2 μM CytoD causes a reduction, by greater than 50%, in the PLCγ1 accumulation for both DNP-BSA and DNP-SLB patterns (Figure 4A, bottom panels, and Figure 4C). These results indicate that stabilization by polymerizing actin is required for PLCγ (but not LAT accumulation) with densely clustered IgE-FcεRI (DNP-BSA). In contrast, stimulated actin polymerization stabilizes the accumulation of both PLCγ and LAT with more sparsely clustered IgE-FcεRI (DNP-SLB).

We tested for PLCγ1 activation in RBL cells on patterned DNP-BSA regions with an antibody specific for the phosphorylated tyrosine residue 783 (pY783). As shown in Figure 4B and quantified in

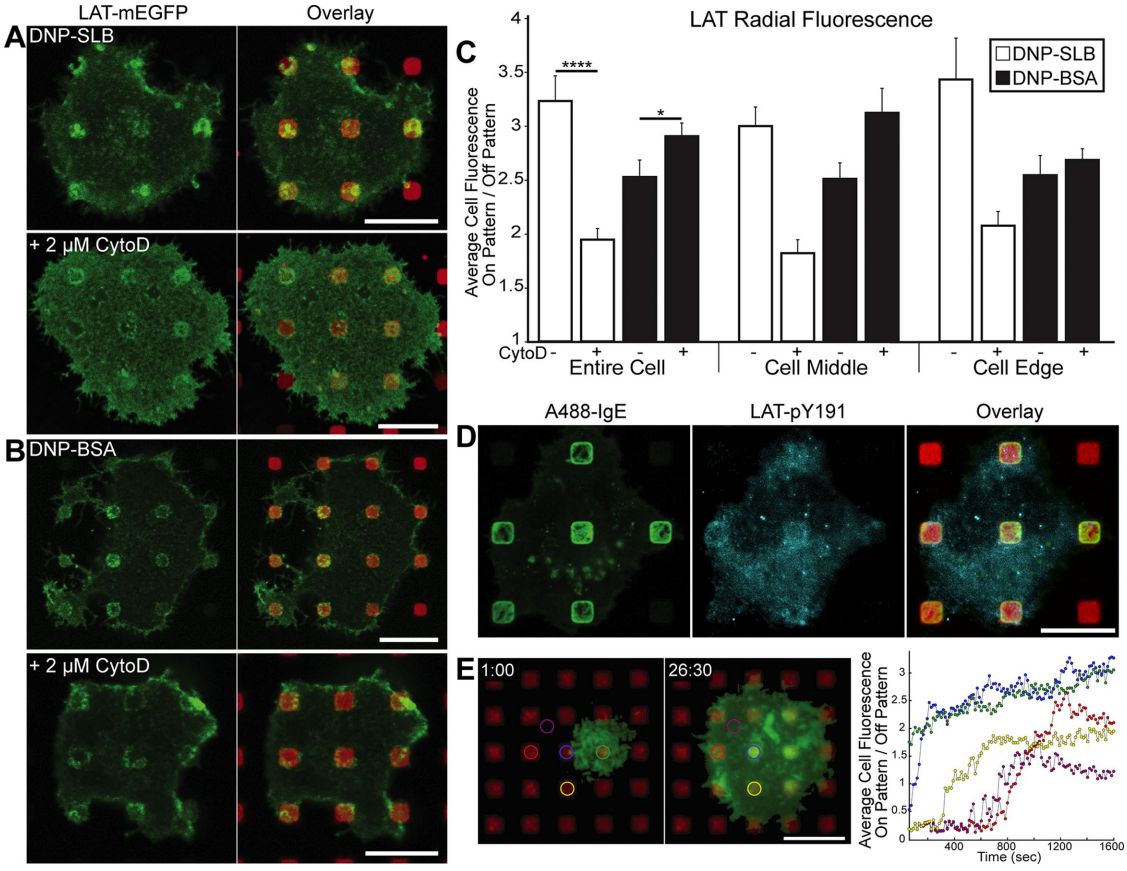

FIGURE 3: LAT recruitment to regions of clustered FcεRI on patterned DNP surfaces is differentially regulated by actin polymerization. RBL cells transiently transfected with LAT-mEGFP (green) and sensitized with IgE were incubated with DNP-SLB– (A) or DNP-BSA–patterned (B) surfaces (red). Cells shown in bottom panels were pretreated with 2 μM CytoD. (C) Radial analysis was carried out as described in the legend to Figure 1. $N = 25$ cells from three independent experiments for each patterned-surface type. Error bars represent SEM; statistical significance: *, $p \leq 0.05$; ****, $p \leq 0.0001$. (D) Cells sensitized with A488-IgE-FcεRI (green) were incubated with DNP-BSA–patterned surfaces and, after fixation, labeled with an antibody specific for LAT-pY191 (cyan). Cell shown is representative of 60% of cells scored as positive for concentrated LAT-pY191 (see *Materials and Methods*). (E) Dynamic TIRF imaging of IgE-sensitized RBL cells transiently transfected with LAT-mEGFP on surfaces with patterned DNP-SLB. Left two panels show the same cell interacting with the surface after 1:00 and 26:30 min (a movie of this cell with time-lapse imaging is supplied as Supplemental Figure 3E Movie). Right panel shows the time-dependent fluorescence ratio of on-versus-off patterned features for LAT-mEGFP, calculated at 15-s intervals for the differently colored ROI circles identified in the left panels. Four circles are placed over patterned features and one circle (magenta) is located off patterned features; increasing fluorescence ratios include contributions from both cell spreading and accumulation of LAT-mEGFP. Scale bars: 10 μm.

Figure 4C, distinct on-feature fluorescence and low off-feature fluorescence characterized the concentration of PLCγ1-pY783 at individual DNP-BSA features for a majority of cells. These results provide evidence that this downstream enzyme, which hydrolyzes PIP_2 to IP_3 and DAG, is recruited to phosphorylated FcεRI and activated, likely as part of a complex with phosphorylated LAT (Rivera and Gilfillan, 2006). Signaling even farther downstream is identifiable at these sites in the form of phosphorylated extracellular signal-regulated kinase (ERK) (Supplemental Figure S6A).

We also tested cells lacking Syk (Syk-negative cells) (Zhang *et al.*, 1996) for FcεRI-stimulated recruitment of PLCγ1 and thereby its dependence on activated Syk (Simon *et al.*, 2005). We observed no concentration of PLCγ1-EGFP to any patterned DNP-BSA surfaces for transfected Syk-negative cells imaged in two separate experiments (Figure 4D, left panel). We generally observed that Syk-negative cells remain largely rounded after the standard incubation conditions, consistent with abrogation of cell spreading in the absence of downstream signaling (Zhang *et al.*, 1996), and we confirmed this with imaging in an equatorial focal plane (Figure 4D, right panel).

Thus our results provide strong evidence that Syk activation and consequent F-actin polymerization are required for stable recruitment of PLCγ1 to clustered FcεRI signaling complexes.

β1-integrins accumulate at DNP-SLB–patterned regions as the result of stimulated trafficking

Previous studies have characterized the interplay between integrin-mediated cell spreading and FcεRI-mediated intracellular signaling when sensitized RBL mast cells interact with antigen on surfaces (Hamawy *et al.*, 1992; Yasuda *et al.*, 1995; Apgar, 1997). We used our patterned ligand surfaces to investigate spatial relationships of clustered/activated FcεRI and integrins that interact with the ECM protein FN. Integrins on RBL cells include VLA-4 (α4β1), VLA-5 (α5β1), and VNR (αVβ3) (Yasuda *et al.*, 1995), with VLA-4 reportedly

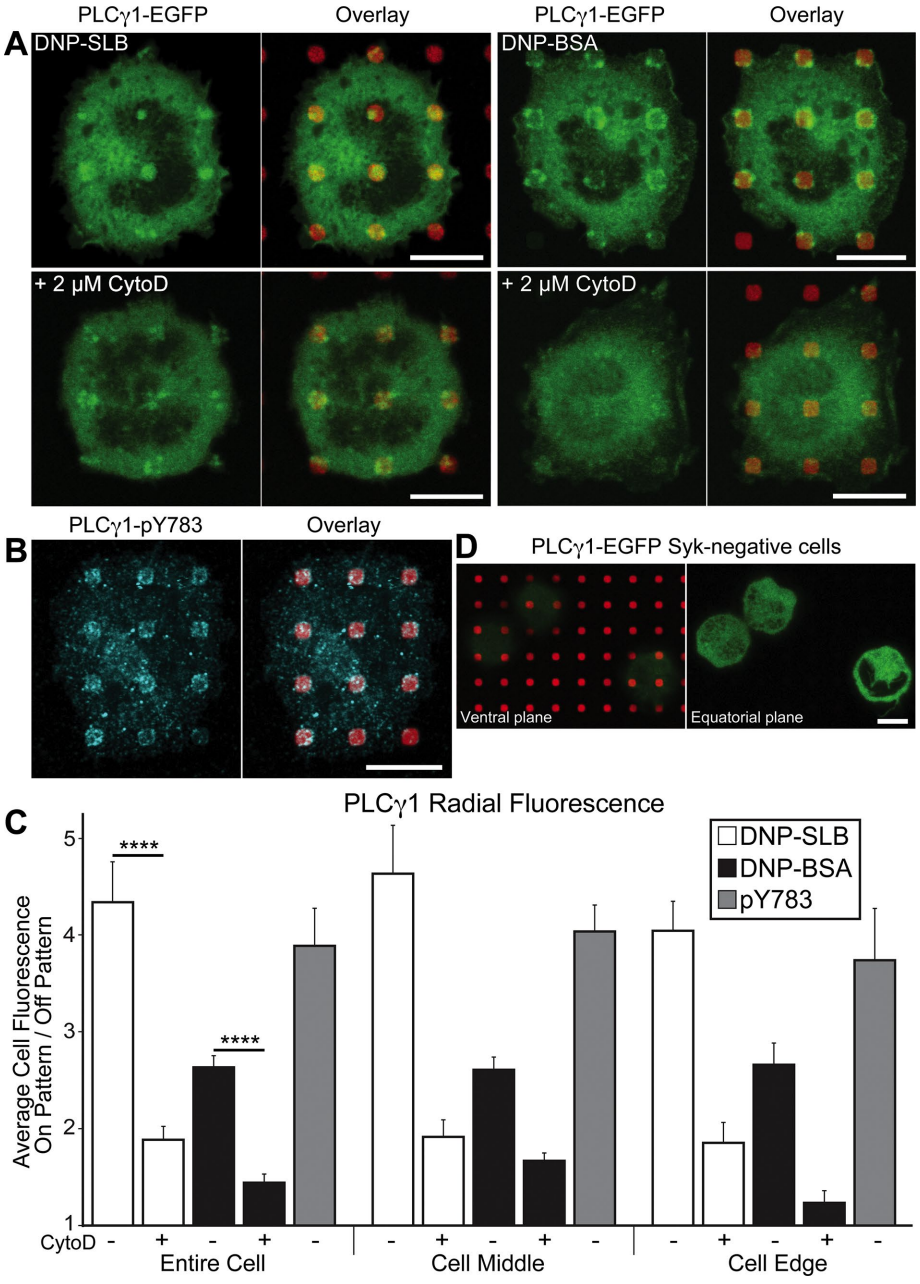

FIGURE 4: Actin polymerization stabilizes PLCγ1 accumulation in regions of clustered FcεRI on DNP-patterned surfaces. (A) RBL cells transiently transfected with PLCγ1-EGFP (green) and sensitized with IgE were incubated on DNP-SLB– (left two panels) and DNP-BSA–patterned (right two panels) surfaces (red). Cells shown in bottom panels were pretreated with 2 μM CytoD. (B) Sensitized cells were incubated on DNP-BSA–patterned surfaces and, after fixation, labeled with an antibody specific for PLCγ1-pY783 (cyan). Cell shown is representative of 90% of cells scored as positive in this sample. (C) Radial analysis (carried out as described in the legend to Figure 1) to quantify PLCγ1-EGFP and PLCγ1-pY783 recruitment to patterned DNP-features. $N = 30$ cells from at least three independent experiments for each sample type. Error bars represent SEM; statistical significance: ****, $p \leq 0.0001$. (D) Syk-negative RBL cells transiently transfected with PLCγ1-EGFP (green) and sensitized with IgE were incubated with DNP-BSA–patterned surfaces (red). Cells shown are representative of all cells transfected with PLCγ1-EGFP observed in two independent experiments; focal planes at cell ventral surface (left panel) or cell equator (right panel). Scale bars: 10 μm.

the most highly expressed (Grodzki *et al.*, 2003). Our experiments tested available monoclonal antibodies specific for integrin subunits: anti-α4 and anti-β3, which are competitive for FN binding (Yasuda *et al.*, 1995). We also used an anti-β1 mAb, which does not block binding to ECM (von Ballestrem *et al.*, 1996; Singhai *et al.*, 2014), unlike the other two antibodies. However, we found that this anti-β1 does not bind after fixing RBL cells, and therefore labeled with this antibody before the fixation of cells already adherent to patterned surfaces. We further evaluated cells transfected with β3-mEGFP. Other integrin-fluorescent protein constructs that we evaluated for this study either did not express well or were mislocated in unstimulated cells under our conditions.

Using the anti-β1 mAb, we observed β1-integrins accumulating at surface-patterned DNP-SLB features in sensitized RBL cells (Figure 5A, left image pair). This clustering, visible in 70% of all cells imaged, predominates at patterned features in contact with the cell edge (Figure 5, A and G, white bars). We did not detect β1 clustering for cells incubated on DNP-BSA–patterned surfaces (Figure 5A, right image pair), suggesting that this configuration of clustered IgE-FcεRI does not recruit this integrin or that the anti-β1 mAb is sterically hindered from binding in this case. Neither the anti-α4 nor the anti-β3 label concentrates in regions of clustered IgE-FcεRI (unpublished data). This result can be explained by recruited α4- and β3-integrins already bound to FN, thereby preventing the binding of these antibodies specific for the same integrin regions (Yasuda *et al.*, 1995).

In cells transfected with β3-mEGFP, we observed recruitment to patterned DNP-SLB regions, with an apparent preference for patterned features located near the cell middle (Supplemental Figure S7, A and B). When FN was covalently coupled as patterned features, we observed some colocalization of β3-mEGFP, and this accumulation was additionally enhanced by stimulation with soluble DNP-BSA (Supplemental Figure S8A). Further, concentrated β3-mEGFP fluorescence was detectable on DNP-BSA–patterned surfaces (Supplemental Figure S8C). Taken together, these results are consistent with the stable recruitment of β1-integrins and β3-integrins to regions where IgE-FcεRI is clustered by DNP-ligands.

We further investigated the possibility that this β1- and β3-integrin recruitment to patterned DNP-SLB regions is due to IgE-FcεRI–stimulated and IgE-FcεRI–targeted trafficking from an intracellular pool. These experiments were motivated by previous studies on integrin trafficking (Pierini *et al.*, 2000; Pellinen *et al.*, 2006; Caswell *et al.*, 2008) and also by our previous observations of IgE-FcεRI–stimulated trafficking of cholera toxin subunit B (CTxB) from recycling endosomes (REs; Naal *et al.*, 2003) and the targeting of REs to regions of patterned

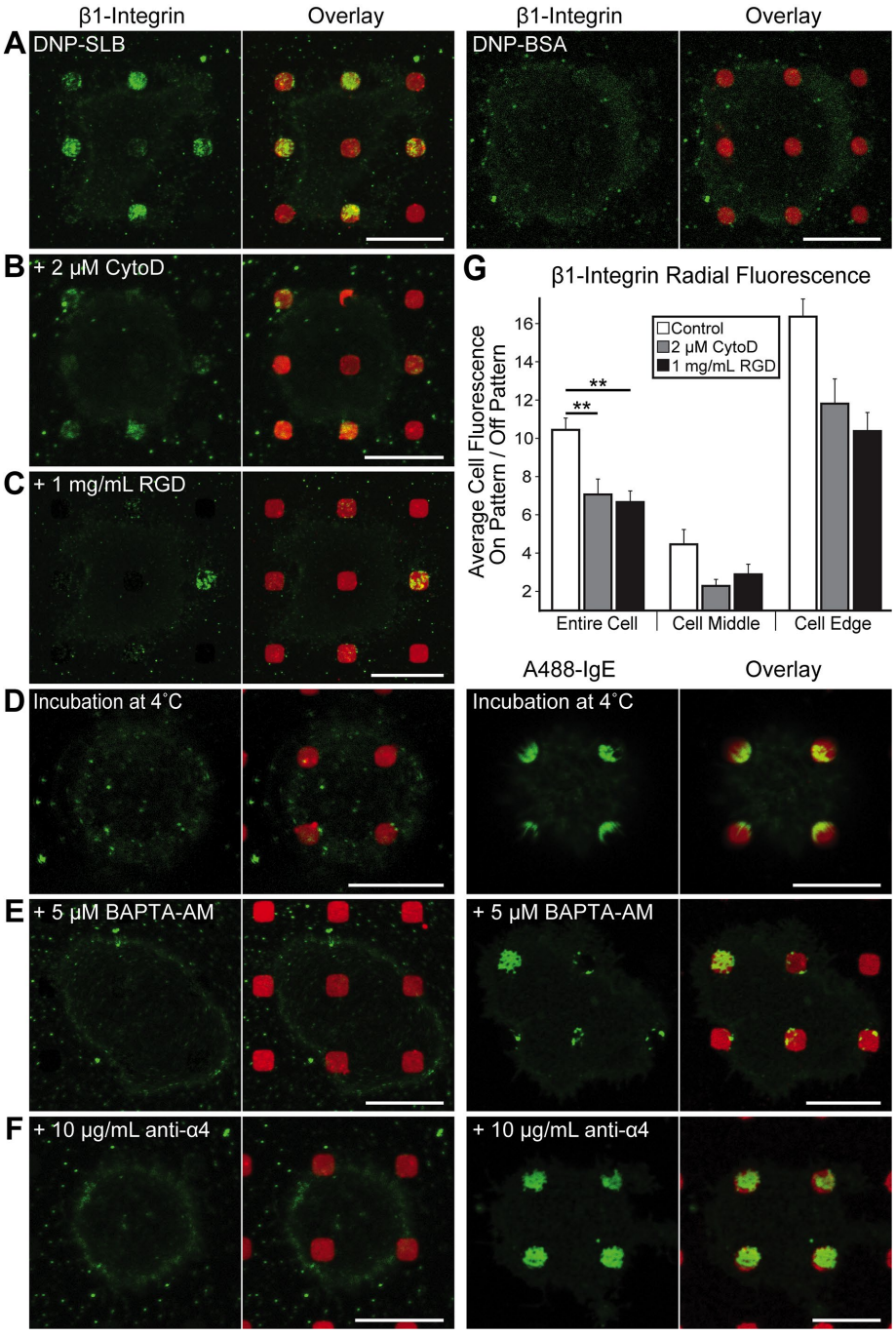

FIGURE 5: β1-Integrin coclusters with IgE-FcεRI on patterned DNP-SLB in an active process that depends on actin polymerization and intracellular Ca^{2+}. (A) Sensitized RBL cells were labeled with anti-β1 mAb (green) after incubation at 37°C on patterned features of DNP-SLB (red, left pair) or DNP-BSA (red, right pair). (B) Same as left pair in A, except that cells were pretreated with 2 μM CytoD. (C) Same as left pair in A, except that cells were incubated on patterned DNP-SLB surfaces in the presence of 1.5 μM RGD peptide. (D) Sensitized cells incubated at 4°C on patterned DNP-SLB (red) surfaces and labeled with anti-β1 (green, left pair) or A488-IgE (green, right pair). (E) Sensitized cells pretreated with 5 μM BAPTA-AM, incubated at 37°C on patterned DNP-SLB (red) surfaces and labeled with anti-β1 (green, left pair) or A488-IgE (green, right pair). (F) Sensitized cells pretreated with 10 μg/ml anti-α4 mAb, incubated at 37°C on patterned DNP-SLB (red) surfaces and labeled with anti-β1 (green, left pair) or A488-IgE (green, right pair). (G) Radial analysis for samples represented in A–C (carried out as described in the legend to Figure 1) quantify β1-integrin recruitment to DNP-SLB features. $N = 30$ cells from three independent experiments for each sample type. Error bars represent SEM; statistical significance: **, $p \leq 0.01$. Scale bars: 10 μm.

ligand (Wu *et al.*, 2007). We found that the accumulation of β1-integrin does not occur if cells are incubated with patterned surfaces at 4°C instead of at 37°C (compare Figure 5, A and D, left image pairs). IgE-FcεRI still concentrates at patterned sites, and its reduced accumulation at 4°C (Figure 5D, right image pair) may be due in part to the cells remaining more rounded under these conditions. Our results are consistent with the requirement of higher temperatures for intracellular trafficking, including our previous finding that CTxB targeted to DNP-presenting features occurs at the higher but not the lower temperature (Wu *et al.*, 2007). We also tested the effects of chelating intracellular Ca^{2+} to suppress Ca^{2+} mobilization stimulated by clustered FcεRI and required for stimulated exocytosis of REs (Naal *et al.*, 2003). For this purpose, we pretreated sensitized cells with 5 μM BAPTA-AM before their incubation on patterned substrates in Ca^{2+}-free buffer. This treatment resulted in more rounded cells, prevented the accumulation of β1-integrins with DNP-SLB features (Figure 5E, left image pair), and reduced the concentration of IgE-FcεRI in these regions (Figure 5E, right image pair).

We investigated the presence of an intracellular pool of integrins by comparison with CTxB, which labels the plasma membrane of RBL cells and internalizes into REs that localize to the perinuclear region (Naal *et al.*, 2003). Because the anti-β1 mAb does not bind after cells are fixed, we monitored β1-integrins in the form of VLA-4 (α4β1) and used the anti-α4 mAb (Yasuda *et al.*, 1995) in these experiments. IgE-sensitized cells labeled with Alexa Fluor 555 (A555)-CTxB and subsequently fixed, permeabilized, and labeled with anti-α4 mAb revealed a prominent perinuclear pool of REs containing both CTxB and α4-integrins (Figure 6A, top panels). Stimulation of these A555-CTxB–labeled cells with soluble DNP-BSA before fixing and labeling with anti-α4 resulted in decreased fluorescence for both CTxB and α4-integrin in the perinuclear RE pool (Figure 6A, bottom panels). The simultaneous appearance of bright puncta in the cytoplasm, containing both CTxB and α4-integrin, is consistent with REs in the process of outward trafficking. To quantify the extent of CTxB and α4-integrin trafficking, we calculated the fluorescence ratio of the perinuclear RE pool to the total cell fluorescence. Stimulation with DNP-BSA caused an average decrease of 25% in perinuclear CTxB fluorescence and a 35% decrease in perinuclear α4-integrin fluorescence (Figure 6C). This reduction is consistent with outward

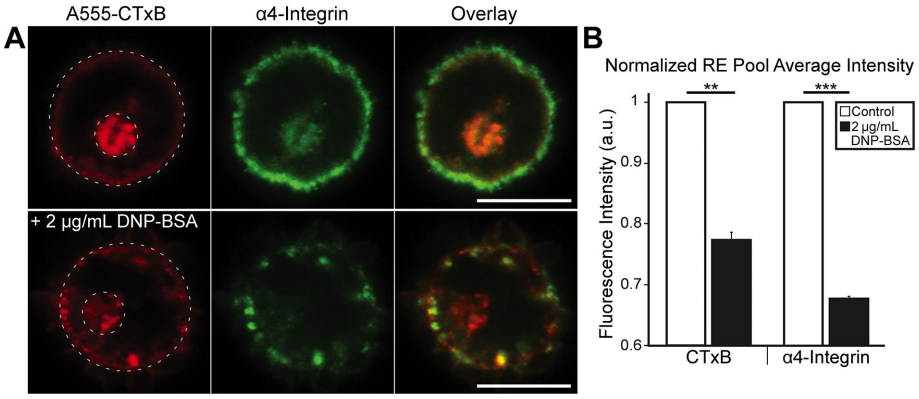

FIGURE 6: CTxB and α4-integrin colocalize with REs in RBL cells. (A) Sensitized cells were labeled with A555-CTxB (red) and not stimulated (top) or stimulated with 2 μg/ml DNP-BSA for 10 min (bottom) and then fixed, permeabilized, and labeled with anti-α4 mAb (green). (B) The normalized average fluorescence intensity for the RE pool (smaller dotted circle in A) is divided by the total cell fluorescence (larger dotted circle) for CTxB and α4-integrin, with and without DNP-BSA stimulation. $N = 23$ cells from three independent experiments for each sample type. Error bars represent SEM; statistical significance: **, $p \leq 0.01$; ***, $p \leq 0.001$. Scale bars: 10 μm.

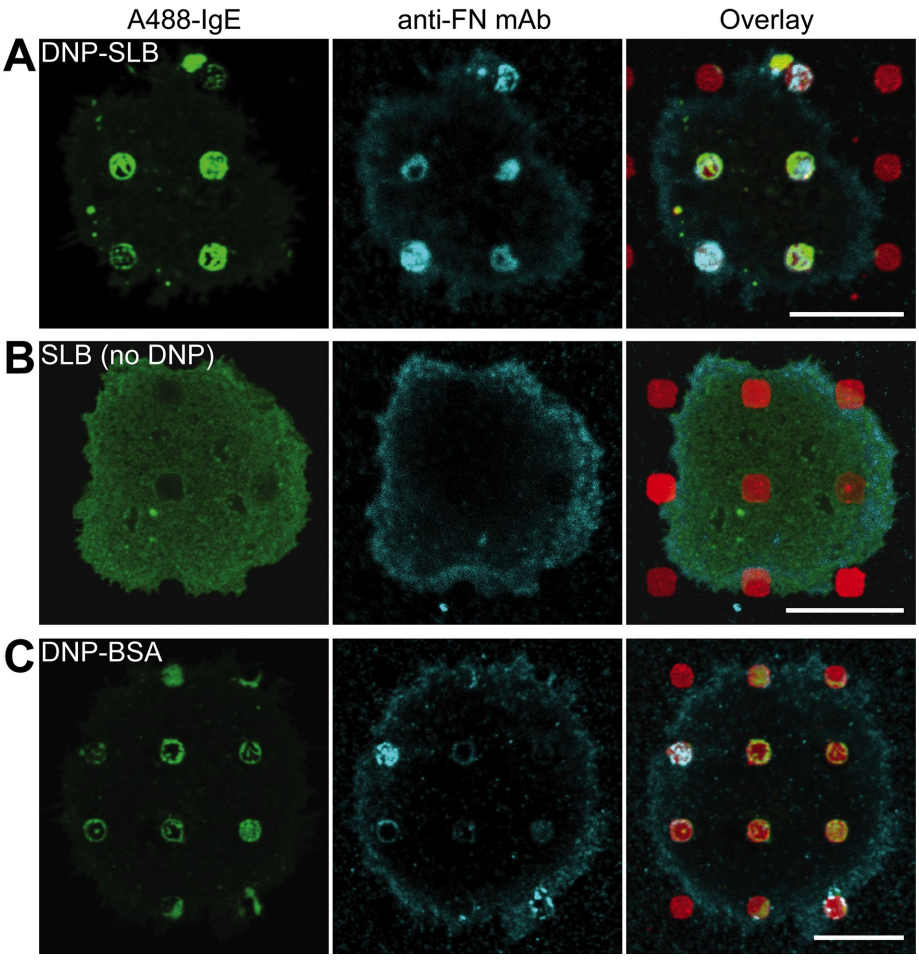

FIGURE 7: FN concentrates with clustered IgE-FcεRI at patterned DNP-SLB features. (A) A488-IgE (green) sensitized RBL cells were incubated at 37°C on DNP-SLB (red) patterned surfaces, then fixed and immunolabeled for FN (cyan). (B) Same as A, except that patterned features were SLBs without DNP-cap-DPPE. (C) A488-IgE–sensitized (green) RBL cells were incubated at 37°C on DNP-BSA–patterned surfaces (red), then fixed and immunolabeled for FN (cyan). Scale bars: 10 μm.

trafficking of REs stimulated by soluble DNP-BSA and with the accumulation of α4β1-integrin with DNP-SLB-patterned features (Figure 5A). We obtained similar results with β3-integrin using RBL cells transfected with the β3-mEGFP (Supplemental Figure S7C).

Trafficking and stabilization of β1-integrins with clustered IgE-FcεRI depends on F-actin and FN binding

We evaluated other intra- and extracellular factors regulating β1-integrin accumulation with clustered IgE-FcεRI on patterned DNP-SLB. Treating the cells with 2 μM CytoD before incubation with patterned substrates caused a 30% decrease in the clustering of β1-integrin across the entire cell (Figure 5, B and G). We observed a similarly reduced accumulation when cells were pretreated with 1.5 μM of the FN peptide GRGDSPC (RGD) (Figure 5, C and G). After pretreating the cells with anti-α4 mAb, which blocks integrin binding to FN, we found that sensitized cells remained rounded, β1-integrins did not accumulate in these regions (Figure 5F, left image pair), and IgE-FcεRI still clustered at patterned DNP-SLB sites (Figure 5F, right image pair). A likely explanation for these results is that clustered IgE-FcεRI stimulates β1-integrins in REs to traffic to regions of clustered IgE-FcεRI, where they are exocytosed and cross-linked by extracellular FN. These integrin complexes are then further stabilized in patterned regions by their intracellular linkages to the actin cytoskeleton.

This explanation assumes that FN is present in the regions of clustered IgE-FcεRI where β1-integrins are exocytosed. The only source of FN would be from the cells themselves, and we tested the possibility that FN is also trafficked to patterned sites simultaneously with the stimulated trafficking of integrins. Using immunofluorescence, we found that trafficked FN colocalized with patterned DNP-SLB features and clustered IgE-FcεRI in 70% of the cells imaged (Figure 7A). This colocalization did not occur when cells were incubated at 4°C instead of 37°C, similar to the suppression of β1-integrin trafficking (Figure 5D). When DNP was omitted from the patterned SLBs, we observed IgE-FcεRI exclusion (as in Figure 1B) and diffuse anti-FN labeling across the ventral surface (Figure 7B). Sensitized cells incubated with patterned DNP-BSA also showed relatively diffuse labeling for FN, with limited concentration of FN fluorescence at patterned sites (Figure 7C). This result is consistent with the lack of detectable β1-integrin labeling under these conditions (Figure 5A, right image pair) and may be related to antibody access in these labeling schemes or to

differential trafficking. These results support the hypothesis that IgE-FcεRI, clustered by patterned DNP-SLB, initiates Syk-mediated signaling pathways and stimulates the outward trafficking of both β1-integrins and FN. Both components are exocytosed in regions of clustered IgE-FcεRI, and integrins, cross-linked by FN, are stabilized in these regions via intracellular connections to the actin cytoskeleton. Inhibition of these signaling and trafficking events prevents cells from spreading and decreases the engagement of the cell membrane with the substrate.

DISCUSSION

Spatial regulation of IgE receptor–mediated signaling

We used patterned ligand surfaces to gain new information about IgE-FcεRI–mediated targeting of signaling complexes and processes, and our findings have clear implications for other cellular systems. Our patterned ligand approach provides the opportunity to examine the redistribution of signaling components with respect to the localization of engaged receptors, and features of micrometer dimension readily lend themselves to robust fluorescence imaging and quantitative analysis. Although this approach does not directly discern nanoscale assemblies that may be sufficient to initiate signaling physiologically, the increased area of receptor engagement stabilizes subtle and/or transient signaling interactions that would otherwise be difficult to detect. We characterized IgE-FcεRI–mediated recruitment of early signaling components Lyn, Syk, LAT, and PLCγ1 and found that stimulated actin polymerization is increasingly involved in stabilizing this sequential assembly of signaling complexes. Activation of PLCγ1 leads to Ca^{2+} mobilization, which is required for stimulated exocytosis of secretory granules and REs. We determined that both β1-integrins and their FN ligands are stimulated to traffic from an intracellular pool of REs and are targeted to exocytose at patterned regions of clustered receptors as cell spreading proceeds.

We evaluated patterned features of either mobile (DNP-SLB) or immobilized (DNP-BSA) ligands and observed distinctive patterns of IgE-FcεRI recruitment in RBL mast cells associating with these surfaces. A relatively dense presentation of immobilized DNP-BSA concentrates IgE-FcεRI at the patterned feature edges with limited diffusion to the interior, whereas IgE-FcεRI is more uniformly distributed across mobile DNP-SLB–patterned features. Our radial analysis method quantifies these differences both in terms of on-versus-off feature fluorescence intensity ratios (different levels of recruitment) and in terms of the variation of these ratios for patterned features at cell edges versus the cell middle (differential spatial targeting).

We previously showed that Lyn kinase is recruited to IgE-FcεRI clustered on DNP-SLB–patterned surfaces, resulting in robust tyrosine phosphorylation in these regions (Wu *et al.*, 2004). In the present study, we found that the tyrosine kinase Syk and the scaffolding protein LAT also show the same redistributions to patterned features as clustered IgE-FcεRI, which are distinctive for the DNP-SLB and DNP-BSA surfaces. Interestingly, we found that Syk recruitment occurs to a similar extent whether or not actin polymerization is inhibited by CytoD (Figure 2). These results confirm that cytoskeletal stabilization is unnecessary for receptor-mediated recruitment of Lyn and Syk to initiate downstream signaling. Our recent superresolution fluorescence localization microscopy revealed that both nanoscale coclustering of antigen–cross-linked IgE-FcεRI with Lyn and separately with the saturated acyl membrane anchor of Lyn are slightly enhanced in the presence of CytoD or latrunculin A (Shelby *et al.*, 2016). Results from these and other complementary approaches support the view that coupling of Lyn with clustered IgE-FcεRI occurs in ordered lipid regions of the plasma membrane (Holowka and Baird, 2015).

LAT is a substrate for Syk at multiple tyrosine sites and consequently acts as a scaffold to assemble multiple adaptor and signaling proteins, including PLCγ1, in hematopoietic cells. Phosphorylated LAT also connects to the actin cytoskeleton via WASP, Arp2/3, and other pathways (Koretzky *et al.*, 2006; Kumari *et al.*, 2014). With an antibody specific for LAT pY191, we showed that LAT recruited to clustered IgE-FcεRI is phosphorylated. We found that LAT accumulates with IgE-FcεRI clustered at high density at the edges of DNP-BSA features, in the absence or presence of CytoD, whereas LAT recruitment to DNP-SLB is 50% reduced by this inhibitor. These results indicate that IgE-FcεRI that is either immobilized or densely packed (as with the DNP-BSA features) couples with Lyn, Syk, and LAT without additional stabilization by the actin cytoskeleton. In contrast, LAT recruitment to IgE-FcεRI complexes clustered by the less dense, mobile ligand in DNP-SLB features is enhanced by actin polymerization after initial LAT phosphorylation.

Interestingly, we found that detectable recruitment of PLCγ1 to regions of clustered IgE-FcεRI is inhibited by CytoD for both DNP-BSA and DNP-SLB features, indicating a higher level of stimulated actin polymerization is required to stabilize the LAT-mediated signaling complexes at this stage. We further showed that this recruited PLCγ1 is phosphorylated on Y783, confirming activation under these conditions. In contrast, we found that PLCγ1 is not recruited to clustered IgE-FcεRI for cells deficient in Syk (Figure 4D), as expected if signaling does not proceed to LAT phosphorylation and consequent assembly of downstream signaling complexes. These results are consistent with the possibility that nucleation of actin polymerization by the LAT-Gads-SLP76-Nck-WASP-Arp2/3 pathway is responsible for stabilizing LAT-scaffolded signaling complexes that lead to PLCγ1 recruitment/activation and consequent Ca^{2+} mobilization, required for downstream FcεRI-stimulated cellular responses (Silverman *et al.*, 2006). Overall our results are consistent with those of Pivniouk *et al.* (2003), who showed, with bone marrow–derived mast cells from WASP-deficient mice, that IgE-dependent activation of PLCγ and Ca^{2+} mobilization leading to degranulation and cytokine secretion are markedly diminished in the absence of WASP. They also found that upstream signaling events, including tyrosine phosphorylation of FcεRI and Syk, are not affected in these WASP-deficient cells. Our results in RBL mast cells are also consistent with those of Kumari *et al.* (2015), who characterized cytoskeletal regulation of T-cell receptor (TCR)-mediated activation of PLCγ1 and Ca^{2+} mobilization in the form of actin foci that assemble via the LAT-scaffolded WASP and Arp2/3 pathway and that associate with TCR microclusters and LAT-mediated signaling complexes.

Stimulated trafficking of β1-integrins to regions of clustered IgE-FcεRI enhances cell spreading on surfaces

Attachment to ligand-presenting surfaces or cells can modulate mast cell responses to specific chemical signals and orient these responses (Hamawy *et al.*, 1992; Carroll-Portillo *et al.*, 2015; Joulia *et al.*, 2015). In previous studies, we found that degranulation of secretory lysosomes in RBL cells occurs toward a ligand-patterned surface, although not directly at regions of ligand-clustered IgE-FcεRI. However, we found that stimulated exocytosis of REs containing internalized CTxB (Naal *et al.*, 2003) occurs preferentially to those same clustered IgE-FcεRI regions (Wu *et al.*, 2007). Our present studies have revealed that surface-patterned ligands additionally stimulate and target the trafficking of α4β1- and β3-integrins from an intracellular pool identified as REs (Figure 6).

We showed that β1-integrin trafficking is targeted preferentially to DNP-SLB features that are closest to the cell edges (Figure 5). This is consistent with integrin-mediated spreading occurring at the leading edge of migrating hematopoietic cells, such as neutrophils (Pierini *et al.*, 2000), although a stimulus distributed across RBL cell surfaces causes them to spread peripherally in all directions (Apgar, 1997). We previously observed similar peripheral targeting of β1-integrins stimulated by clustered EGF receptors on NIH-3T3 cells (Singhai *et al.*, 2014), consistent with this being a more general phenomenon. We also observed that β3-integrins are recruited, with a slight preference for patterned features in the cell middle, suggesting differential targeting mechanisms for different types of integrins (Morgan *et al.*, 2009).

Integrin trafficking has been described for other cell types (Bretscher, 1992; Pierini *et al.*, 2000) and implicated in processes of cell motility and chemotaxis (Pierini *et al.*, 2000). We previously showed that IgE-FcεRI–mediated chemotaxis to antigen in RBL cells depends on Ca^{2+} influx via the plasma membrane channel, Orai1 (Lee *et al.*, 2012). We hypothesize that this Ca^{2+} mobilization is required for integrin trafficking to sites at which FcεRI engages ligand and thereby facilitates chemotactic movement in the direction of a ligand gradient. Recruitment of β1-integrins to patterned DNP-SLB features does not occur in the absence of activating ligand and is inhibited by low temperatures and BAPTA-AM (1,2-*bis*(*o*-aminophenoxy)ethane-*N*,*N*,*N*′,*N*′-tetraacetic acid tetra(acetoxymethyl) ester), which suppresses stimulated Ca^{2+} mobilization (Figure 5).

Unexpectedly, we found that FN is stimulated to co-traffic from intracellular stores to DNP-SLB features where IgE-FcεRI is clustered (Figure 7). It appears that integrins and FN associate at the time of simultaneous exocytosis, because pretreating cells with RGD peptides or with anti-α4 mAb, both of which inhibit integrin–FN association, significantly reduces the accumulation of α4β1 with clustered IgE-FcεRI (Figure 5). We hypothesize that these exocytosed, FN–cross-linked integrins connect to the actin cytoskeleton, which provides an anchor and prevents diffusion away from the regions of clustered receptors. This anchorage also appears to enhance the engagement of IgE-FcεRI with patterned ligands for spreading cells (Figure 5). Our results provide an explanation for RBL cell interactions with surfaces: these cells undergo constitutive recycling of endosomes containing α4β1 and FN, promoting cell adherence on any surface to which FN sticks (Torres *et al.*, 2008; Chiang *et al.*, 2011). IgE-FcεRI–mediated stimulation of signaling pathways, leading to Ca^{2+} mobilization in these adherent cells, causes trafficking and exocytosis of α4β1 and FN in regions of clustered receptors at the cell periphery, resulting in cell spreading and mechanically enhanced signaling.

Our results with RBL cells on patterned ligand surfaces provide insight into studies of other primary and cultured mast cells that migrate and interact specifically with other cells as part of immune responses. For example, integrin αLβ2 (LFA-1) was found to assist in mast cell homing to sites of inflammation and forming aggregates with other inflammatory cells (Weber *et al.*, 1997; Inamura *et al.*, 1998). More recently, Choi *et al.* (2016) showed that, during cystitis, shedding of infected bladder epithelial cells is preceded by targeted recruitment, docking, and degranulation of mast cells. Carroll-Portillo *et al.* (2015) demonstrated that FcεRI-mediated activation of mast cells triggers stable interactions with immature dendritic cells, forming a synapse via mast cell LFA-1 and α4β1, to facilitate material transfer to these dendritic cells. Joulia *et al.* (2015) showed that mast cells with IgE-FcεRI (or immunoglobulin G [IgG]-FcγRIIA) interact with ligand-targeted cells to create an "antibody-dependent degranulatory synapse." Here the mast cell interface was characterized by punctate pTyr and pLAT, polarized exocytosis of granules, and sustained exposure of effector enzymes at the cell–cell contact site. Although Joulia *et al.* (2015) did not examine the participation of integrins in their characterization of this mast cell synapse, other studies described in this paragraph point to α4β1 and LFA-1 involvement. Our characterization of RBL cells reveals underlying mechanisms that are consistent with these previous observations of mast cell activities: directional activation of IgE-FcεRI on a surface causes localized assembly of signaling components, resulting in enhanced cell adherence and targeted exocytosis of integrins and other material.

In summary, our results provide evidence that the clustering of FcεRI by IgE engagement with micron-scale patterned ligands stimulates the recruitment of activated PLCγ1, as well as upstream proteins LAT and Syk, in a complex that depends on stabilization by polymerized actin. In consequently stimulated downstream events, REs containing integrins and their ligand, FN, undergo net outward trafficking and exocytosis that is targeted to clustered IgE-FcεRI, thus promoting active cell spreading. This process we have characterized in RBL mast cells may be more generally relevant to cell chemotaxis toward a ligand gradient and functional engagement with target cells.

MATERIALS AND METHODS

Materials

All cell culture reagents, as well as Alexa Fluor 568 (A568)-streptavidin, A647-phalloidin, A647-labeled goat anti-rabbit IgG, A647-labeled goat anti-mouse IgGγ1, A488-labeled donkey anti-rat IgG, and A555-CTxB were purchased from Invitrogen. FuGENE HD came from Promega. Mouse anti-FN and fluorescein isothiocyanate (FITC)-labeled mouse anti-rat CD49d (anti–α4-integrin) (Yasuda *et al.*, 1995) were purchased from BD Biosciences. Anti-mouse/rat CD61 (anti–β3-integrin) was obtained from Affymetrix and was used to label cells as previously described (Yasuda *et al.*, 1995). FITC-labeled rat anti-CD29 (anti–β1-integrin) was obtained from Millipore. Anti–phospho-Y783-PLCγ1 and rabbit anti-pERK were purchased from Cell Signaling. Anti–phospho-Y191-LAT was purchased from Abcam. A488-IgE was prepared by modification of purified mouse monoclonal anti-DNP IgE (Liu *et al.*, 1980) with A488 (Invitrogen) as previously described (Larson *et al.*, 2005).

DNP sulfonate (Sigma-Aldrich) was conjugated to BSA, similar to the previously described method (Torres *et al.*, 2008), for a yield of ~22 DNP per BSA. DNP-BSA was subsequently conjugated with Cy3 NHS-ester (GE Healthcare) for fluorescence visualization in some experiments. Briefly, in pH 8.5 borate-buffered saline (200 mM boric acid, 33 mM NaOH, and 160 mM NaCl), the amine-reactive Cy3 and DNP-BSA were incubated in the recommended ratio overnight in the dark at room temperature. The reaction mixture was extensively dialyzed against pH 7.4 phosphate-buffered saline (PBS) with 1 mM EDTA to remove unbound dye and was spectroscopically measured to have 2–3 Cy3 molecules per DNP-BSA.

The YFP-Syk cDNA construct was a gift from T. Meyer (Stanford University). The cDNA construct of PLCγ1-EGFP was a gift from G. Carpenter (Vanderbilt University; Wang *et al.*, 2001). The LAT-mEGFP cDNA was prepared and used as described elsewhere (Sengupta *et al.*, 2008). The β3-integrin–mEGFP cDNA construct (Tsuruta *et al.*, 2002) was a gift from A. Kusumi (Kyoto University).

The 1,2-dipalmitoyl-sn-glycero-3-phosphoethanolamine-*N*-[6-[(2,4-dinitrophenyl)amino]hexanoyl] (DNP-cap-DPPE), 1-palmitoyl-2-oleoyl-*sn*-glycero-3-phosphocholine (POPC), 1,2-dioleoyl-*sn*-glycero-3-phosphoethanolamine-*N*-(lissamine rhodamine B sulfonyl) (LissRhod DOPE), and 1,2-dioleoyl-*sn*-glycero-3-phosphoethanolamine-*N*-(7-nitro-2-1,3-benzoxadiazol-4-yl) (NBD DOPE) were

purchased from Avanti Polar Lipids. The RGD peptide, GRGDSPC, was obtained from Phoenix Pharmaceuticals. CytoD was purchased from Calbiochem (EMD Chemicals). Rhodamine-FN (Rhod-FN) was a gift from J. Erickson (Cornell University, originally purchased from Cytoskeleton). BSA, bovine FN, sulfinpyrazone, BAPTA-AM, (3-mercaptopropyl)trimethoxysilane (MPTS), and N-(γ-maleimidobutyryloxy) succinimide ester (GMBS) were purchased from Sigma-Aldrich. Fused silica 100-mm-diameter wafers of coverslip 1.5 thickness (<200 µm thickness) and silicon 100-mm-diameter wafers of standard thickness were purchased from Precision Glass & Optics (PG&O).

Cell culture and transfection

RBL-2H3 cells were maintained as monolayer cultures in MEM containing 20% (vol/vol) fetal bovine serum (FBS) and 50 µg/ml gentamicin. Cells were harvested using trypsin-EDTA (Invitrogen) 3–5 d after passage, as previously described (Pierini *et al.*, 1996). For chemical transfection, a complex of 1–2 µg of cDNA with 8 µl FuGENE HD in 100 µl of Opti-MEM was added to plated cells in 1 ml of Opti-MEM per 35-mm dish for 1 h, followed by the addition of phorbol dibutyrate (0.1 µg/ml) for 4 h. Cells were returned to full serum medium for overnight culture. RBL cells deficient in Syk (Syk-negative cells, TB1A2 cell line; Zhang *et al.*, 1996) were maintained and transfected under the same conditions as described for RBL-2H3 cells.

Fabrication and chemical modification of parylene-patterned surfaces

The preparation of parylene-patterned surfaces has been previously described by our lab (Wu *et al.*, 2004; Singhai *et al.*, 2014) as based on a polymer lift-off technique (Ilic and Craighead, 2000). Briefly highlighting the specific process used in this work (Supplemental Figure S1), fused silica (glass) or silicon wafers were first coated with a 1-µm-thick layer of parylene-C (diX C parylene dimer [Kisco] and an SCS Labcoter Parylene Deposition System), then an ~40-nm-thick layer of antireflective coating (AR3 DUV Anti-Reflectant, Shipley), and finally, a 1-µm-thick layer of photoresist (UV210; Dow Chemical, and Suss MicroTec Gamma Cluster Tool). Using a predesigned photomask and exposure to 248-nm light (ASML PAS 5500/300C DUV Stepper), multiple patterned arrays were created in the photoresist layer. An oxygen-based reactive-ion etch (Oxford 81 Etcher) transferred the features from the patterned photoresist to the underlying parylene layer. Through this etching step, exposed regions of substrate masked by the parylene were made available for chemical modification and the presentation of selected biomaterial, including ligands for specific receptors. Parylene-patterned wafers and/or individually cut parylene-patterned pieces (≤1-cm squares) were stored in a desiccator until ready for chemical modification.

Either immobilized protein or SLBs were used to present receptor ligand on these patterned substrates. For preparation of the substrates for surface functionalization and protein attachment (Supplemental Figure S1, step 6), individual patterned pieces were sequentially rinsed with acetone, isopropanol, and water and dried under nitrogen gas. A brief (~30 s) oxygen plasma cleaning (Harrick Plasma Basic Plasma Cleaner) of patterned substrates was immediately followed by treatment with 4% (vol/vol) MPTS in toluene for 30 min at room temperature. Substrates were then washed with absolute ethanol (three times) and incubated in 2 mM GMBS in absolute ethanol for 30 min at room temperature (Torres *et al.*, 2008). After being rinsed with absolute ethanol several times, these patterns could be stored at 4°C, in absolute ethanol, and sealed with parafilm, up to several months.

Continuing with protein attachment, each patterned substrate was quickly rinsed with PBS (pH 7.4), placed on parafilm, and incubated with 25 µg/ml protein ligand (e.g., Cy3-DNP-BSA or Rhod-FN in PBS) for 2 h at room temperature or overnight at 4°C. After being rinsed with PBS, the parylene was peeled away using tweezers. Subsequent rinsing with PBS to remove any additional pieces of unattached parylene yielded patterned ligand surfaces ready for cell experiments (Supplemental Figure S1, step 8). Protein patterns were stored in PBS with 0.01% sodium azide at 4°C.

Preparation of small unilamellar lipid vesicles and SLBs

Patterned SLBs were alternatively used to present DNP, as shown on the right in Supplemental Figure S1 and as previously described (Torres *et al.*, 2008). The different lipids (POPC, DNP-Cap-DPPE, and LissRhod-DOPE) in chloroform were first mixed at a composition of 89.9:10:0.2 mol%, respectively. After this mixture was dried with a stream of nitrogen gas, the lipid film was then placed under vacuum for >1 h to ensure complete evaporation of the solvent. The dried lipid sample was then resuspended in Tris buffer (50 mM Tris and 200 mM NaCl, pH 8) and subjected to several minutes of vortexing. The hydrated lipid mixture was placed in an ice bath and probe sonicated (Sonics & Materials) for ~15 min or until transparent to obtain small unilamellar vesicles (SUVs). Brief centrifugation and an Acrodisc syringe filter (0.2-µm pore) were then used to remove any particulate in the SUV suspension. SUVs were stored at 4°C under nitrogen gas and sealed with parafilm and used within ~3 wk of preparation.

SLB surfaces were prepared via SUV fusion (Richter *et al.*, 2003). A short oxygen plasma cleaning (Harrick Plasma Basic Plasma Cleaner) was used to establish hydrophilic parylene-patterned surfaces. A sufficient volume of SUVs was then incubated on the surfaces for 15 min, after which time rinsing with an excess of DI water removed any unfused lipid vesicles. Ensuring that the surfaces were not exposed to air during or after this step was crucial to subsequent experimental steps. Peeling the parylene away using tweezers and a final rinsing with more DI water established patterned DNP-SLB surfaces (Supplemental Figure S1, step 7). Experiments with cells were carried out on the same day as SLB preparation.

BSA (1 mg/ml, without DNP) was used in all experiments to limit nonspecific binding to the surfaces surrounding patterned features. We also tested the possibility of passivating this area around patterned regions by backfilling with an SLB (Supplemental Figure S2). However, this level of blocking also prevented cell attachment in these regions, resulting in very few cells adhering to these surfaces. As described in *Results*, this can be explained by cell-secreted FN not sticking to highly passivated surfaces, thereby preventing integrin-mediated cell attachment.

Cell incubation on patterns, immunolabeling, and fluorescence microscopy

RBL cells were harvested and resuspended in balanced salt solution (BSS) with 1 mg/ml BSA at ~0.5×10^6 cells/ml (BSS: 135 mM NaCl, 5.0 mM KCl, 1.8 mM $CaCl_2$, 1.0 mM $MgCl_2$, 5.6 mM glucose, and 20 mM HEPES, pH 7.4). After sensitization with 3 µg/ml IgE or A488-IgE, for 30 min at 37°C, cells were washed and allowed to settle on DNP-patterned surfaces previously blocked with 1 mg/ml BSA. An ~40 min incubation at 37°C was typically followed by fixation with 4% paraformaldehyde and 0.1% glutaraldehyde in PBS for 10 min and multiple washes with 1 mg/ml BSA in PBS.

For immunofluorescence, fixed cells were labeled with primary antibody (5–10 µg/ml) at room temperature for 1 h in PBS with

10 mg/ml BSA. If cytoplasmic labeling was needed, 0.1% Triton X-100 was added with the antibody. After additional washing, fluorescent secondary antibody (5–10 μg/ml) in PBS with 10 mg/ml BSA was added to the samples at room temperature for an additional hour. A final series of PBS washes were used before storing samples in PBS, with 0.01% sodium azide, before microscopic imaging. For F-actin labeling, fixed cells were incubated with 5 μg/ml A647-phalloidin in PBS (10 mg/ml BSA) with 0.1% Triton X-100 for 20 min at room temperature before being rinsed with PBS.

The RBL cell epitope for anti–β1-integrin antibody binding was found to be sensitive to aldehyde fixation, and therefore was used to label cells before fixation. Following incubation at 37°C, cells on patterned surfaces were placed on ice, and primary and secondary antibody labeling in BSS/BSA was performed for 30 min each, washing with BSS/BSA between these labeling steps. Cells were then fixed as described earlier.

In experiments buffering intracellular Ca^{2+}, cells were preloaded with BAPTA-AM (5 μM) in BSS/BSA with 0.5 mM sulfinpyrazone (to prevent leakage of hydrolyzed BAPTA-AM) for 30 min at 37°C. Subsequent incubation of the cells on DNP-patterned surfaces was carried out in Ca^{2+} free BSS buffer with sulfinpyrazone (Figure 5E).

For live-cell imaging of LAT-mEGFP, cells were sensitized with IgE, resuspended in imaging buffer, and pipetted onto the patterned surfaces, which were already placed on the microscope. With a sufficiently high concentration (>10^6 cells/ml), single cells could be identified within the initial minute of settling on the patterned surface (Figure 3E).

Silicon chips with adherent fixed cells were inverted in a coverslip glass-bottom 35-mm dish for imaging. Samples were imaged on a Zeiss LSM 710 inverted microscope with a motorized stage using a 63× oil Plan-Apochromat objective lens. A DF 488/561/647 filter set was used to perform sequential 1/2/3 color imaging of the samples. For collecting YFP fluorescence, an HFT 458/514 filter set was used for imaging. The area of the focal plane was adjusted for optimal image quality.

Owing to variation in fluorescent protein expression, specific criteria were set to provide consistency in the imaging and analysis of cells expressing a particular FcεRI signaling molecule. Cells were not imaged if the target protein was visibly localized to endoplasmic reticulum structures or clearly over/underexpressed (seen as brighter or dimmer fluorescence than average). Cells showing very little or no protein recruitment were still imaged as long as they did not exhibit any of these eliminating properties. For a cell to be scored positive for recruitment of a specific protein, a minimum of two patterned features had to show fluorescence distinguishable from the surrounding cell fluorescence.

Radial analysis of fluorescence colocalization

Our method for quantifying recruitment of fluorescently labeled cellular components to micron-sized patterned features of ligand (DNP-SLB or DNP-BSA) is based on a series of image operations in MATLAB (MathWorks), as illustrated in Supplemental Figures S3 and S4. First, a polygonal region of interest (ROI) was drawn around a single imaged cell to exclude any adjacent cells or any partial patterned features found at the image field-of-view border. This same ROI, applied to the pattern image (Supplemental Figure S3, step 1), was used to localize the centers of each patterned DNP feature. Patterned feature localization was readily accomplished by determining the center-to-center distance and improved through the application of a common MATLAB pixel-intensity edge-detection algorithm (e.g., a Sobel filter). Features not in contact with the cell and any features not within the preset region of analysis (entire cell, cell middle, or cell edge) were manually selected for exclusion at this first step (red slashes). Patterned features were identified as cell middle or cell edge according to the following criteria: "cell edge" patterned features are those that make contact with the boundary of the cell and/or are not completely surrounded by cell background fluorescence to within the distance of another patterned feature size (e.g., a distance of 2 μm). All other patterned features are counted as "cell middle." "entire cell" counts all "cell edge" and "cell middle" patterned features. Patterned features localized to the cell middle were quantified as illustrated in Supplemental Figure S3. Following patterned feature selection, individual features were then grouped together to generate an average pattern feature image (step 2). Using these selected pattern features, the same operation was performed on the fluorescence corresponding to the specific cell response (e.g., recruited A488-IgE-FcεRI; step 3) to establish an average cell response image (step 4). Next the pixel intensities for each of the average pattern feature or average cell response images were plotted as a function of the distance from the patterned feature center (small blue circle shown in steps 2 and 4) to beyond its edge (steps 5 and 6). The patterned feature edge was determined from the average pattern feature image (step 2) and defined as the point midway between the on- and off-feature fluorescence intensities (dotted line derived in step 5 and applied to step 6). As described in *Results* and illustrated in Supplemental Figures S3 and S4, the cell response fluorescence intensities (e.g., A488-IgE-FcεRI) are distinctive for DNP-BSA compared with DNP-SLB–patterned features. Concentrated fluorescence overlapping the defined edge of DNP-BSA features was included in the pixel intensity associated with the patterned feature for quantifying the cell fluorescence ratio value for the average cell response: the mean intensity of the on pattern region (extending from the blue circle center to the green circle in step 4, corresponding to the green line in step 6) was divided by the mean intensity of the off pattern region (extending beyond the red circle in step 4, corresponding to the red line in step 6). This set of image operations was repeated for multiple cells, and the on-versus-off fluorescence intensity ratios were averaged into an overall mean to generate bar graph results, as shown in Figures 1–5 and Supplemental Figures S7 and S9. Quantifying patterned features localized to the cell edge followed the same procedure, except that an additional step was taken to orient patterned features to avoid including fluorescence beyond the cell boundary (Supplemental Figure S4).

ACKNOWLEDGMENTS

This work was supported by the National Institutes of Health (NIH) (R01-AI018306 followed by R01-GM117552). We appreciate experimental resources provided by the Cornell NanoScale Science and Technology Facility (National Science Foundation [NSF] ECCS-1542081) and the Cornell Biotechnology Resource Center Imaging Facility, including the Zeiss LSM 710 confocal microscope (NIH S10RR025502) and Zeiss Elyra superresolution microscope (NSF 1428922). The content is solely the responsibility of the authors and does not necessarily represent the official views of the NSF or NIH.

REFERENCES

Andrews NL, Lidke KA, Pfeiffer JR, Burns AR, Wilson BS, Oliver JM, Lidke DS (2008). Actin restricts FcεRI diffusion and facilitates antigen-induced receptor immobilization. Nat Cell Biol 10, 955–963.

Apgar JR (1991). Regulation of the antigen-induced F-actin response in rat basophilic leukemia cells by protein kinase C. J Cell Biol 112, 1157–1163.

Apgar JR (1997). Increased degranulation and phospholipase A2, C, and D activity in RBL cells stimulated through FcεRI is due to spreading and not simply adhesion. J Cell Sci 110, 771–780.
Barker SA, Caldwell KK, Pfeiffer JR, Wilson BS (1998). Wortmannin-sensitive phosphorylation, translocation, and activation of PLCγ1, but not PLCγ2, in antigen-stimulated RBL-2H3 mast cells. Mol Biol Cell 9, 483–496.
Bretscher MS (1992). Circulating integrins: α5β1, α6β4 and Mac-1, but not α3β1, α4β1 or LFA-1. EMBO J 11, 405–410.
Carroll-Portillo A, Cannon JL, te Riet J, Holmes A, Kawakami Y, Kawakami T, Cambi A, Lidke DS (2015). Mast cells and dendritic cells form synapses that facilitate antigen transfer for T cell activation. J Cell Biol 210, 851–864.
Caswell PT, Chan M, Lindsay AJ, McCaffrey MW, Boettiger D, Norman JC (2008). Rab-coupling protein coordinates recycling of α5β1 integrin and EGFR1 to promote cell migration in 3D microenvironments. J Cell Biol 183, 143–155.
Chiang EN, Dong R, Ober CK, Baird BA (2011). Cellular responses to patterned poly(acrylic acid) brushes. Langmuir 27, 7016–7023.
Choi HW, Bowen SE, Miao YX, Chan CY, Miao EA, Abrink M, Moeser AJ, Abraham SN (2016). Loss of bladder epithelium induced by cytolytic mast cell granules. Immunity 45, 1258–1269.
Draber P, Sulimenko V, Draberova E (2012). Cytoskeleton in mast cell signaling. Front Immunol 3, 1–18.
Finco TS, Kadlecek T, Zhang WG, Samelson LE, Weiss A (1998). LAT is required for TCR-mediated activation of PLCγ1 and the Ras pathway. Immunity 9, 617–626.
Frigeri L, Apgar JR (1999). The role of actin microfilaments in the down-regulation of the degranulation response in RBL-2H3 mast cells. J Immunol 162, 2243–2250.
Gaudenzio N, Sibilano R, Marichal T, Starkl P, Reber LL, Cenac N, McNeil BD, Dong XZ, Hernandez JD, Sagi-Eisenberg R, *et al.* (2016). Different activation signals induce distinct mast cell degranulation strategies. J Clin Invest 126, 3981–3998.
Grodzki ACG, Pastor MVD, Sousa JF, Oliver C, Jamur MC (2003). Differential expression of integrin subunits on adherent and nonadherent mast cells. Braz J Med Biol Res 36, 1101–1109.
Hamawy MM, Oliver C, Mergenhagen SE, Siraganian RP (1992). Adherence of rat basophilic leukemia (RBL-2H3) cells to fibronectin-coated surfaces enhances secretion. J Immunol 149, 615–621.
Hernandez-Hansen V, Smith AJ, Surviladze Z, Chigaev A, Mazel T, Kalesnikoff J, Lowell CA, Krystal G, Sklar LA, Wilson BS, *et al.* (2004). Dysregulated FcεRI signaling and altered Fyn and SHIP activities in Lyn-deficient mast cells. J Immunol 173, 100–112.
Holowka D, Baird B (2015). Nanodomains in early and later phases of FcεRI signalling. Essays Biochem 57, 147–163.
Holowka D, Calloway N, Cohen R, Gadi D, Lee J, Smith NL, Baird B (2012). Roles for Ca^{2+} mobilization and its regulation in mast cell functions. Front Immunol 3, 1–10.
Holowka D, Sheets ED, Baird B (2000). Interactions between FcεRI and lipid raft components are regulated by the actin cytoskeleton. J Cell Sci 113, 1009–1019.
Ilic B, Craighead HG (2000). Topographical patterning of chemically sensitive biological materials using a polymer-based dry lift off. Biomed Microdevices 2, 317–322.
Inamura N, Mekori YA, Bhattacharyya SP, Bianchine PJ, Metcalfe DD (1998). Induction and enhancement of FcεRI-dependent mast cell degranulation following coculture with activated T cells: dependency on ICAM-1- and leukocyte function-associated antigen (LFA)-1-mediated heterotypic aggregation. J Immunol 160, 4026–4033.
Joulia R, Gaudenzio N, Rodrigues M, Lopez J, Blanchard N, Valitutti S, Espinosa E (2015). Mast cells form antibody-dependent degranulatory synapse for dedicated secretion and defence. Nat Commun 6.
Kimura T, Hisano M, Inoue Y, Adachi M (2001). Tyrosine phosphorylation of the linker for activator of T cells in mast cells by stimulation with the high affinity IgE receptor. Immunol Lett 75, 123–129.
Kimura T, Sakamoto H, Appella E, Siraganian RP (1996). Conformational changes induced in the protein tyrosine kinase p72(syk) by tyrosine phosphorylation or by binding of phosphorylated immunoreceptor tyrosine-based activation motif peptides. Mol Cell Biol 16, 1471–1478.
Koretzky GA, Abtahian F, Silverman MA (2006). SLP76 and SLP65: complex regulation of signalling in lymphocytes and beyond. Nat Rev Immunol 6, 67–78.
Kumari S, Curado S, Mayya V, Dustin ML (2014). T cell antigen receptor activation and actin cytoskeleton remodeling. Biochim Biophys Acta 1838, 546–556.
Kumari S, Depoil D, Martinelli R, Judokusumo E, Carmona G, Gertler FB, Kam LC, Carman CV, Burkhardt JK, Irvine DJ, *et al.* (2015). Actin foci facilitate activation of the phospholipase C-γ in primary T lymphocytes via the WASP pathway. eLife 4, e04953.
Larson DR, Gosse JA, Holowka DA, Baird BA, Webb WW (2005). Temporally resolved interactions between antigen-stimulated IgE receptors and Lyn kinase on living cells. J Cell Biol 171, 527–536.
Lee J, Veatch SL, Baird B, Holowka D (2012). Molecular mechanisms of spontaneous and directed mast cell motility. J Leukocyte Bio 92, 1029–1041.
Liu FT, Bohn JW, Ferry EL, Yamamoto H, Molinaro CA, Sherman LA, Klinman NR, Katz DH (1980). Monoclonal sinitrophenyl-specific murine IgE antibody: preparation, isolation, and characterization. J Immunol 124, 2728–2737.
Menon AK, Holowka D, Webb WW, Baird B (1986). Cross-linking of receptor-bound IgE to aggregates larger than dimers leads to rapid immobilization. J Cell Biol 102, 541–550.
Metcalfe DD, Baram D, Mekori YA (1997). Mast cells. Physiol Rev 77, 1033–1079.
Morgan MR, Byron A, Humphries MJ, Bass MD (2009). Giving off mixed signals-distinct functions of α5β1 and αVβ3 integrins in regulating cell behaviour. IUBMB Life 61, 731–738.
Naal RMZG, Holowka EP, Baird B, Holowka D (2003). Antigen-stimulated trafficking from the recycling compartment to the plasma membrane in RBL mast cells. Traffic 4, 190–200.
Orth RN, Wu M, Holowka DA, Craighead HG, Baird BA (2003). Mast cell activation on patterned lipid bilayers of subcellular dimensions. Langmuir 19, 1599–1605.
Pellinen T, Arjonen A, Vuoriluoto K, Kallio K, Fransen JAM, Ivaska J (2006). Small GTPase Rab21 regulates cell adhesion and controls endosomal traffic of β1-integrins. J Cell Biol 173, 767–780.
Pierini L, Holowka D, Baird B (1996). FcεRI-mediated association of 6-μm beads with RBL-2H3 mast cells results in exclusion of signaling proteins from the forming phagosome and abrogation of normal downstream signaling. J Cell Biol 134, 1427–1439.
Pierini LM, Lawson MA, Eddy RJ, Hendey B, Maxfield FR (2000). Oriented endocytic recycling of α5β1 in motile neutrophils. Blood 95, 2471–2481.
Pivniouk VI, Snapper SB, Kettner A, Alenius H, Laouini D, Falet H, Hartwig J, Alt FW, Geha RS (2003). Impaired signaling via the high-affinity IgE receptor in Wiskott-Aldrich syndrome protein-deficient mast cells. Int Immunol 15, 1431–1440.
Richter RP, Him JLK, Brisson A (2003). Supported lipid membranes. Mater Today 6, 32–37.
Rivera J, Gilfillan AM (2006). Molecular regulation of mast cell activation. J Allergy Clin Immunol 117, 1214–1225; quiz 1226.
Saitoh S, Arudchandran R, Manetz TS, Zhang W, Sommers CL, Love PE, Rivera J, Samelson LE (2000). LAT is essential for FcεRI-mediated mast cell activation. Immunity 12, 525–535.
Sengupta P, Hammond A, Holowka D, Baird B (2008). Structural determinants for partitioning of lipids and proteins between coexisting fluid phases in giant plasma membrane vesicles. Biochim Biophys Acta 1778, 20–32.
Shelby SA, Holowka D, Baird B, Veatch SL (2013). Distinct stages of stimulated FcεRI receptor clustering and immobilization are identified through superresolution imaging. Biophys J 105, 2343–2354.
Shelby SA, Veatch SL, Holowka DA, Baird BA (2016). Functional nanoscale coupling of Lyn kinase with IgE-FcεRI is restricted by the actin cytoskeleton in early antigen-stimulated signaling. Mol Biol Cell 27, 3645–3658.
Silverman MA, Shoag J, Wu J, Koretzky GA (2006). Disruption of SLP-76 interaction with Gads inhibits dynamic clustering of SLP-76 and FcεRI signaling in mast cells. Mol Cell Biol 26, 1826–1838.
Simon M, Vanes L, Geahlen RL, Tybulewicz VLJ (2005). Distinct roles for the linker region tyrosines of Syk in FcεRI signaling in primary mast cells. J Biol Chem 280, 4510–4517.
Singhai A, Wakefield DL, Bryant KL, Hammes SR, Holowka D, Baird B (2014). Spatially defined EGF receptor activation reveals an F-actin-dependent phospho-Erk signaling complex. Biophys J 107, 2639–2651.
Torres AJ, Vasudevan L, Holowka D, Baird BA (2008). Focal adhesion proteins connect IgE receptors to the cytoskeleton as revealed by micropatterned ligand arrays. Proc Natl Acad Sci USA 105, 17238–17244.
Tsuruta D, Gonzales M, Hopkinson SB, Otey C, Khuon S, Goldman RD, Jones JCR (2002). Microfilament-dependent movement of the β3 integrin subunit within focal contacts of endothelial cells. FASEB J 16, 866–868.
von Ballestrem CG, Uniyal S, McCormick JI, Chau T, Singh B, Chan BMC (1996). VLA-β1 integrin subunit-specific monoclonal antibodies MB1.1

and MB1.2: binding to epitopes not dependent on thymocyte development or regulated by phorbol ester and divalent cations. Hybridoma 15, 125–132.
Wang XJ, Liao HJ, Chattopadhyay A, Carpenter G (2001). EGF-dependent translocation of green fluorescent protein-tagged PLC-γ1 to the plasma membrane and endosomes. Exp Cell Res 267, 28–36.
Weber S, Babina M, Feller G, Henz BM (1997). Human leukaemic (HMC-1) and normal skin mast cells express beta 2-integrins: characterization of beta 2-integrins and ICAM-1 on HMC-1 cells. Scand J Immunol 45, 471–481.
Wu M, Baumgart T, Hammond S, Holowka D, Baird B (2007). Differential targeting of secretory lysosomes and recycling endosomes in mast cells revealed by patterned antigen arrays. J Cell Sci 120, 3147–3154.
Wu M, Holowka D, Craighead HG, Baird B (2004). Visualization of plasma membrane compartmentalization with patterned lipid bilayers. Proc Natl Acad Sci USA 101, 13798–13803.
Yamada KM (1991). Adhesive recognition sequences. J Biol Chem 266, 12809–12812.
Yasuda M, Hasunuma Y, Adachi H, Sekine C, Sakanishi T, Hashimoto H, Ra C, Yagita H, Okumura K (1995). Expression and function of fibronectin binding integrins on rat mast cells. Int Immunol 7, 251–258.
Zhang J, Berenstein EH, Evans RL, Siraganian RP (1996). Transfection of Syk protein tyrosine kinase reconstitutes high affinity IgE receptor-mediated degranulation in a Syk-negative variant of rat basophilic leukemia RBL-2H3 cells. J Exp Med 184, 71–79.
Zhang WG, Irvin BJ, Trible RP, Abraham RT, Samelson LE (1999). Functional analysis of LAT in TCR-mediated signaling pathways using a LAT-deficient Jurkat cell line. Int Immunol 11, 943–950.
Zhang WG, Trible RP, Zhu MH, Liu SK, McGlade J, Samelson LE (2000). Association of Grb2, Gads, and phospholipase C-γ1 with phosphorylated LAT tyrosine residues. J Biol Chem 275, 23355–23361.